Journal of Molecular and Cellular Cardiology Plus 7 (2024) 100059

Contents lists available at ScienceDirect

Journal of Molecular and Cellular Cardiology Plus

journal homepage: www.journals.elsevier.com/journal-of-molecular-andcellular-cardiology-plus

Sacubitril/valsartan reduces proteasome activation and cardiomyocyte area in an experimental mouse model of hypertrophy

Moritz Meyer-Jens [a,b,1], Kristin Wenzel [c,d,1], Karina Grube [c,d], Julia Rüdebusch [c,d], Elisabeth Krämer [a,b], Martin Bahls [c,d], Kilian Müller [e], Hannah Voß [e], Hartmut Schlüter [e], Stephan B. Felix [c,d], Lucie Carrier [a,b], Stephanie Könemann [c,d,2], Saskia Schlossarek [a,b,2,*]

[a] Institute of Experimental Pharmacology and Toxicology, University Medical Center Hamburg-Eppendorf, Martinistr. 52, 20246 Hamburg, Germany
[b] German Centre for Cardiovascular Research (DZHK), partner site Hamburg/Kiel/Lübeck, Germany
[c] Department of Internal Medicine B, University Medicine Greifswald, Sauerbruchstraße, 17475 Greifswald, Germany
[d] German Centre for Cardiovascular Research (DZHK), partner site Greifswald, Germany
[e] Section Mass Spectrometric Proteomics, University Medical Center Hamburg-Eppendorf, Martinistr. 52, 20246 Hamburg, Germany

ARTICLE INFO

Keywords:
Autophagy-lysosomal pathway
Cardiac function
Heart failure
Pressure overload
Sacubitril/valsartan
Ubiquitin-proteasome system

ABSTRACT

Sacubitril/valsartan (Sac/Val) belongs to the group of angiotensin receptor–neprilysin inhibitors and has been used for the treatment of heart failure (HF) for several years. The mechanisms that mediate the beneficial effects of Sac/Val are not yet fully understood. In this study we investigated whether Sac/Val influences the two proteolytic systems, the ubiquitin-proteasome system (UPS) and the autophagy-lysosomal pathway (ALP), in a mouse model of pressure overload induced by transverse aortic constriction (TAC) and in human induced pluripotent stem cell-derived cardiomyocytes (hiPSC-CMs) treated with endothelin-1 (ET1) serving as a human cellular model of hypertrophy. TAC mice showed a continuous decline in cardiac function starting from day 14 after surgery. Administration of Sac/Val for 6 weeks counteracted the deterioration of cardiac function and attenuated hypertrophy and fibrosis in TAC mice. The expression of ALP key markers did not differ between the groups. Proteasome activity was higher in TAC mice and normalized by Sac/Val. In hiPSC-CMs, all treatments (Sac, Val or Sac/Val) normalized mean cell area. However, Sac alone or in combination with Val, but not Val alone prevented ET1-induced hypertrophic gene program and proteomic changes. In conclusion, Sac/Val normalized proteasome activity, improved cardiac function and reduced fibrosis and hypertrophy in TAC mice. Molecular analysis in hiPSC-CMs suggests that a major part of the beneficial effects of Sac/Val is derived from the Sac action rather than from Val.

1. Introduction

Heart failure (HF) is the leading cause of mortality worldwide. The progression of HF is driven by processes such as hypertrophy and fibrosis which then lead to a reduction in cardiac function. Sacubitril-valsartan (Sac/Val), formerly known as LCZ696, represents an angiotensin receptor-neprilysin inhibitor (ARNI) that is indicated for the treatment of patients with symptomatic HF with reduced ejection fraction [1]. The neutral endopeptidase neprilysin degrades several endogenous vasoactive peptides, including natriuretic peptides, bradykinin, and adrenomedullin [2–4]. Natriuretic peptides convey various cardioprotective properties partly by antagonizing the renin-angiotensin-aldosterone system at many levels [5]. Inhibition of neprilysin leads to higher levels of natriuretic vasoactive peptides which counteracts vasoconstriction, sodium retention, and maladaptive remodeling [6,7]. Angiotensin receptor blockade by valsartan in combination with neprilysin inhibition by sacubitril was shown to achieve a decrease in left atrial size and a greater improvement of NYHA class than valsartan alone in HF patients [8]. In the setting of the PARADIGM-HF (Prospective Comparison of ARNI with ACEI to Determine Impact on Global

* Corresponding author at: Institute of Experimental Pharmacology and Toxicology, University Medical Center Hamburg-Eppendorf, Martinistrasse 52, 20246 Hamburg, Germany.
E-mail address: s.schlossarek@uke.de (S. Schlossarek).
[1] Shared first authorship.
[2] Shared last authorship.

https://doi.org/10.1016/j.jmccpl.2023.100059
Received 3 November 2023; Received in revised form 28 December 2023; Accepted 30 December 2023
Available online 7 January 2024

Mortality and Morbidity in Heart Failure) trial, clinically stable patients with HF were treated with Sac/Val or enalapril [9,10]. In this population the use of Sac/Val resulted in a lower risk of death from cardiovascular causes or hospitalization for HF than the use of enalapril. In 2016, the use of the new compound was endorsed by an updated guideline of the American College of Cardiology-American Heart Association [11]. The PIONEER-HF (Comparison of Sacubitril-Valsartan Versus Enalapril on Effect on NT-proBNP in Patients Stabilized From an Acute Heart Failure Episode) trial investigated the use of Sac/Val in patients that were hospitalized for acute decompensated HF [12]. In this study treatment with Sac/Val after hemodynamic stabilization led to a greater reduction in NT-proBNP levels than enalapril treatment [12].

In cardiomyocytes, as terminally differentiated cells, protein quality control is crucial for maintaining cellular homeostasis. The two main proteolytic mechanisms for ensuring protein quality control are the ubiquitin-proteasome system (UPS) and the autophagy-lysosomal pathway (ALP). Degradation of misfolded and/or damaged proteins by the UPS occurs via an ATP-dependent, strictly regulated and highly selective multistep process and involves the (poly)ubiquitination of a target protein through a series of enzymatic reactions and the subsequent degradation of this (poly)ubiquitinated protein by the 26S proteasome [13,14]. Degradation of aggregated proteins and dysfunctional organelles by the ALP involves the formation of a double-membrane vesicle, termed autophagosome, which subsequently fuses with a lysosome to form an autolysosome, in which the cargo is degraded by lysosomal proteases [15]. A growing body of evidence suggests that deviation from appropriate levels of protein quality control, reflected in an altered UPS and ALP function, may be involved in cardiac diseases, such as dilated and hypertrophic cardiomyopathies [16–20]. While a marked accumulation of (poly)ubiquitinated proteins has been shown as a common feature of cardiac disorders [21–23], higher or lower proteasomal activities have been reported depending on the status of the cardiac disease [22–27]. Autophagy has been identified as a mediator of HF [28,29]. The angiotensin II type 1 receptor (AT1R) blocker losartan reduced autophagy and improved cardiac function in rats suffering from severe burns [30]. Since the effect of ARNI on UPS and ALP has not been examined yet, we investigated in the present study whether Sac/Val influences these two proteolytic systems in a mouse model of transverse aortic constriction (TAC) and, in the further course, in a human induced pluripotent stem cell (hiPSC)-derived cardiomyocyte model of hypertrophy.

2. Material and methods

2.1. Ethics statement

All experimental procedures were conducted in compliance with the national guidelines of the German animal protective law for the use of laboratory animals. All animal procedures conform to the guidelines of Directive 2010/63/EU of the European Parliament on the protection of animals used for scientific purposes. The protocols used were approved by the local animal care committee (Landesamt für Landwirtschaft, Lebensmittelsicherheit und Fischerei Mecklenburg-Vorpommern; LALLF-MV, 7221.3-1-022/17).

2.2. Transverse aortic constriction surgery and animal husbandry

In order to investigate the effect of Sac/Val on the progression of HF and the regulation of UPS and ALP in HF mice the murine model of pressure overload by TAC was used. Hence, 8-week-old male C57BL/6 N mice (Charles River Laboratories, Sulzfeld, Germany) underwent either TAC or sham surgery. For surgery, mice were initially anesthetized with 3 % isoflurane, intubated and ventilated (2 % isoflurane in air, 50 ml/min; rodent MiniVent, Harvard Apparatus, Germany). Median sternotomy to the 3rd rib was used to open the thoracic cavity. Afterwards a blunted needle (26G) was placed on the aortic arch between the innominate artery and the left common carotid and a 7–0 suture was tied onto the needle. Immediately afterwards, the needle was removed, thus ensuring a normalized reduced aortic lumen and the thoracic cavity was closed. The sham surgery was performed the same way but without knotting the suture.

For analgesia, subcutaneous injections of 0.1 mg/kg body weight of buprenorphine (Buprenovet, Bayer HealthCare, Leverkusen, Germany) were administered before surgery and subsequently at 12-h intervals (until the third postoperative day). The animals were housed under standard conditions with a 12-h light-dark cycle and controlled temperature (21 °C) regime. Water and food were provided ad libitum.

2.3. Drug administration

Sac/Val was administered at 12-h intervals starting on day 14 after sham/TAC surgery and continued throughout the trial period. For this purpose, the mice of the Sac/Val groups (sham/TAC) were treated with a total dosage of 114 mg/kg body weight/day in a total volume of 400 µl (2 × 200 µl) water per oral gavage. Control mice (sham/TAC) were given 200 µl of water twice daily. The pure substance was provided by Novartis AG (Basel, Switzerland), the dosage recommendation was based on in-house kinetics studies (data not shown).

2.4. Echocardiography

Transthoracic echocardiography was performed using the Vevo®2100 micro-ultrasound imaging system (FUJIFILM VisualSonics®, Inc., Amsterdam, Netherlands). Anesthesia was induced using 1.5 % isoflurane (Baxter, Deerfield, Il, USA) and the breast area was depilated (Veet, Ricket Benckiser Deutschland GmbH, Heidelberg, Germany). Body temperature, heart rate and respiration rate were continuously monitored and kept constant during the 15 min measurement. For the measurement, the animals were fixed to a warming platform in a supine position. B-mode images were obtained using a MS 400 transducer with a frame rate of 230–400 frames/s. Two-dimensional short axis views were recorded at the mid-papillary muscle level. The dimensions of the left ventricle were measured in a short axis view in diastole and systole. All images were recorded digitally and off-line analysis was performed using the Vevo 2100 software.

2.5. Study design and tissue processing

The animals were randomized into four treatment groups: (1) sham/vehicle (n = 18), (2) sham/Sac/Val (n = 21), (3) TAC/vehicle (n = 16), and (4) TAC/Sac/Val (n = 20). All animals received a baseline echo followed by the corresponding operation (sham or TAC) under anesthesia. The drug or vehicle administration started at day 14 after sham/TAC surgery twice a day. In addition, longitudinal echocardiographic examinations were performed at day 14 (before drug administration), day 35 and day 56 after sham/TAC surgery to determine the progression of the disease according to TAC and the effect of Sac/Val. The end of the trial was reached 8 weeks after surgery. The animals were anesthetized by thiopental injection (i.p. 300 mg/kg body weight) and sacrificed by cervical dislocation. Whole blood and the heart were collected. Heart tissue intended for immunohistochemistry was horizontally sectioned in an upper and a lower part whereby the upper part was fixed immediately in 4 % paraformaldehyde. The lower part as well as the whole heart tissues were stored at −80 °C until further analysis.

2.6. 2D culture of hiPSC-derived cardiomyocytes

The commercially available hiPSC line mTagRFPT-TUBA1B (AICS-0031-035, Coriell Institute, Camdem, NJ, US) was used for the generation of hiPSC-derived cardiomyocytes (hiPSC-CMs). Cells were seeded at a density of 6.5×10^4 hiPSC/cm^2, maintained in homemade medium (DMEM F-12, L-glutamine 2 mM, transferrin 5 µg/ml, selenium 5 ng/ml,

human serum albumin 0.1 %, lipid mixture 1×, insulin 5 μg/ml, dorsomorphin 50 nM, activin A 2.5 ng/ml, TGFβ1 0.5 ng/ml, bFGF 30 ng/ml) with a daily feeding schedule and kept under hypoxic conditions. Moreover, cells were monitored daily and passaged at about 90 % confluency. For this step medium was supplemented with Y-27632 (10 μM). Differentiation of hiPSC to hiPSC-CMs followed a monolayer protocol adapted from [31]. One day prior to the start of this protocol cells were passaged and seeded onto 6-well plates coated with matrigel (Corning, 354,234, high growth factor) at a density of 5.2×10^4 hiPSC/cm^2. The next day cells were fed in the morning and stage 0 medium (StemPro-34 SFM, StemPro Supplement 2.6 %, BMP4 1 ng/ml, L-glutamine 2 mM, matrigel high growth factor 1 %) was added in the evening for mesoderm induction. Starting with the addition of the differentiation medium, cells were kept under normoxic conditions. After 12–16 h medium was changed to stage 1 (stemPro-34 SFM, stemPro supplement 2.6 %, BMP4 10 ng/ml, L-glutamine 2 mM, activin A 8 ng/ml) to induce specification of cardiac progenitor cells. Stage 2.1 (RPMI1640, B27 2 %, KYO2111 10 μM, XAV939 10 μM) and 2.2 medium (stage 2.1 with insulin 3.21 μg/ml) were added after subsequent 48 h time frames for Wnt inhibition. Feeding medium (RPMI1640, B27 5 %, insulin 3.21 μg/ml) was added 48 h after stage 2.2 and then subsequently every other day until the cells were homogenously contracting. After dissociation, hiPSC-CMs (on average 82 % cardiac troponin T (TNNT2)-positive cells) were seeded at low density (20,000 cells per cm^2 culture surface) using complete medium (DMEM, penicillin-streptomycin 1 %, horse serum (inactive) 10 %, insulin 10 μg/ml, aprotinin 33 μg/ml) on geltrex (Gibco A14133–02)-coated culture dishes and kept at 37 °C and 7 % CO_2. After three days in culture, the medium was changed to maturation medium ([32]; DMEM w/o glucose, glucose 3 mM, L-lactate 10 mM, vitamin B12 5 μg/ml, biotin 0.82 μM, creatine monohydrate 5 mM, taurine 2 mM, L-carnitine 2 mM, ascorbic acid 0.5 mM, NEAA 1×, albumax I 0.5 %, B27 1×, Knockout serum replacement 1×, penicillin-streptomycin 1 %, insulin 10 μg/ml), in which the cells were kept for 14 days prior to the experiments with a medium change every five days. For the induction of cellular hypertrophy, 100 nM endothelin-1 (ET1, Sigma Aldrich, 05-23-3800) were used with daily medium changes. The preventive treatments with sacubitrilat (Sac, 40 μM, Sigma Aldrich, SML2064), valsartan (Val, 13 μM, Sigma Aldrich, SML0142) or the combination of both (Sac/Val) were carried out in addition to the ET1 treatment while the control and ET1 only groups contained additional 0.08 % DMSO, which was used as a solvent for Sac and Val.

2.7. RNA isolation and analyses

Total RNA was isolated from powdered whole heart tissue samples using the SV Total RNA Isolation System (Promega, Madison, WI, USA) according to the manufacturer's instructions. From 2D-cultured hiPSC-CMs, total RNA was extracted using TRIzol® Reagent (Thermo Fisher Scientific) following the manufacturer's instructions.

RNA concentration, purity and quality were determined using the NanoDrop® ND-1000 spectrophotometer (Thermo Fisher Scientific). For heart tissue samples, reverse transcription was performed from 200 ng RNA using oligo-dT primers (SuperScript® III First-Strand Synthesis System, Thermo Fisher Scientific).

The quantitative determination of beclin-1 (*Becn1*), microtubule-associated protein 1 light chain 3 (*Map1lc3b*), p62/sequestosome 1 (*Sqstm1*), Rab-7 (*Rab7*), lysosomal-associated membrane protein-2 (*Lamp2*), and guanine nucleotide-binding protein, alpha stimulating *(Gnas)* mRNAs was performed by qPCR using the Maxima™ SYBR Green/ROX qPCR Master Mix (Thermo Fisher Scientific), and primers specific for every mouse sequence (see supplemental Table 1). *Gnas* was used as an endogenous control to normalize the quantification of the target mRNAs for differences in the amount of total RNA added to each reaction. Experiments were performed on the ABI PRISM 7900HT Sequence Detection System (Applied Biosystems). The mRNA amount was estimated according to the comparative Ct method with the $2^{-\Delta\Delta Ct}$ formula.

For further gene expression analysis, customized NanoString's nCounter® Elements TagSet panels were used. About 50 ng RNA of each sample were hybridized to the target-specific capture and reporter probes at 67 °C overnight (16 h) according to manufacturer's instructions. Samples were cooled down to 4 °C, supplemented with 15 μl H_2O, and loaded into the NanoString cartridge. Afterwards the nCounter Gene Expression Assay was started immediately. Raw data were analyzed with the nCounter® Sprint Profiler. Transcript levels were determined with the nSolver™ Data Analysis Software including background subtraction using negative controls and normalization to six housekeeping genes (*Abcf1*, *Actb, Cltc, Gapdh, Pgk1* and *Tubb5* for murine data and *ABCF1, ACTB, CLTC, GAPDH, PGK1* and *TUBB* for human data, respectively). Data represent the mean of normalized RNA counts and are expressed as fold change over sham/vehicle or DMSO control, respectively.

2.8. Sample preparation for Western blot analysis and determination of the 20S chymotrypsin-like activity

Heart tissue samples were powdered, and protein extraction was performed in two steps. First, the organ powder (about 30 mg) was dissolved in 150 μl water with a protease inhibitor cocktail (complete mini™, Roche Diagnostics, Rotkreuz, Switzerland). After three liquid nitrogen freeze-thaw-cycles the tissue was homogenized by using Tissue Lyser (2 × 30 s at 20 Hz) and centrifuged at 4 °C, full speed for 30 min in a table-top centrifuge. The supernatant was kept as the cytosolic fraction. Second, the pellet of the first step was homogenized in 240 μl SDS-buffer (3 % SDS, 30 mM Tris-base, pH 8.8, 5 mM EDTA, 30 mM NaF, 10 % glycerol and 1 mM DTT) and centrifuged at room temperature, full speed for 10 min in a table-top centrifuge. The supernatant was kept as the myofilament-enriched fraction.

For Western blot analysis of 2D-cultured hiPSC-CMs, 100 μl SDS-buffer were added to the cell pellet (obtained from 195,000 cells). The cell lysate was homogenized by pipetting up and down and centrifuged at room temperature, full speed for 10 min in a table-top centrifuge. The supernatant was kept as total crude protein lysate.

For measurement of the chymotrypsin-like activity in 2D-cultured hiPSC-CMs, the cell pellet (obtained from 390,000 cells) was dissolved in 50 μl water with a protease inhibitor cocktail (complete mini™, Roche Diagnostics, Rotkreuz, Switzerland). After three freeze-thaw-cycles the cell lysate was homogenized by pipetting up and down and centrifuged at 4 °C, full speed for 30 min in a table-top centrifuge. The supernatant was kept as the cytosolic fraction.

2.9. Western blot

Proteins of the myofilament-enriched (heart tissue) or crude (cells) fraction were loaded on acrylamide/bisacrylamide (29:1) gels and electrotransferred to nitrocellulose membranes, except for LC3 analysis, for which proteins were electrotransferred to polyvinylidene fluoride membranes. Antibodies against the following proteins were used for Western blot analysis: α-actinin (Sigma Aldrich, A7811), beclin-1 (Cell Signaling Technology, 3738), GAPDH (HyTest, 5G4), LAMP-2 (Abcam, ab13524), LC3 (Cell Signaling Technology, 2775), p62/sequestosome-1 (Sigma Aldrich, P0067), Rab-7 (Sigma Aldrich, R4779), ribosomal protein S6 (Cell Signaling Technology, 2217), and (poly-)ubiquitinated proteins (Enzo Life Sciences, BML-PW8810). Signals were revealed with the Clarity Western ECL substrate (Bio-Rad) and acquired with the ChemiDoc Touch Imaging System (Bio-Rad). Signals were quantified with the Image Lab Software (Bio-Rad).

2.10. Determination of the 20S chymotrypsin-like activity

The 20S chymotrypsin-like activity of the proteasome was assessed in the cytosolic protein fraction as described previously [33]. For

determination of the activity, 30 μg (heart tissue) or 10 μg (cells) of protein were diluted in incubation buffer (20 mM HEPES, 0.5 mM EDTA, 5 mM DTT, 0.1 mg/ml ovalbumin) to a final volume of 50 μl. Samples were pre-incubated in this buffer for 2 h at 4 °C. Following pre-incubation, the synthetic fluorogenic substrate Suc-LLVY-AMC (Enzo Life Sciences, BML—P802) was added to the samples at a final concentration of 60 μM. After incubation in the dark for 1 h at 37 °C, the fluorescence of the released AMC reporter was measured using the TECAN Safire2 microplate reader at an excitation wavelength of 380 nm and an emission wavelength of 460 nm. The value of the blank (incubation buffer only) was subtracted from the value of each sample.

2.11. Immunohistochemistry

For heart histological analyses, the heart was fixed in 4 % paraformaldehyde in phosphate-buffered saline and embedded in paraffin. Tissue slices of 6 μm were stained with Sirius Red (Sigma Aldrich, 43,665) or dystrophin (Sigma Aldrich, D8043). For quantification of the fibrotic area a Biorevo BZ-9000 microscope (Keyence, Osaka, Japan) and BZ-X analyzer software (Keyence) were used. After automated capture of 10× magnified images over the entire tissue sample, a single high-resolution image of the whole heart was created. Cardiac fibrosis was quantified by using the single extraction mode software (BZ-X analyzer software, Keyence), which calculated the results as percent of fibrosis related to the entity of the tissue slice. The severity of cardiomyocyte hypertrophy due to TAC was analyzed using a dystrophin antibody (Sigma Aldrich, D8043) staining and the Biorevo BZ-9000 microscope (Keyence, Osaka, Japan). The quantification of cell size was performed using the ImageJ software (U.S. National Institutes of Health).

2.12. Analysis of cellular hypertrophy

For the analysis of parameters of cellular hypertrophy, hiPSC-CMs were seeded at a density of 2500–5000 cells/well onto a 96-well plate and cultured as described above resulting in singularized cells. After compound treatment, the cells were fixed with 50 μl Roti-Histofix (Carl Roth, P087.5) for 20 min at 4 °C. Before and after the fixation the cells were washed twice with PBS. Cells were stained with an antibody specific for alpha-actinin (Sigma Aldrich, A7811) and Hoechst33342 (Invitrogen, H3570) for visualization of the nuclei. After primary antibody incubation the wells were washed and fluorescently labeled antibodies were added that matched the species of the primary counterparts.

Z-stack images of the cells were taken using a Zeiss LSM800 system. The lower and upper limit of the stack was determined using the alpha-actinin signal (stained with secondary antibody AF488). Each slice was 0.29 μm thick. In the analysis process the threshold was adjusted in a way that this signal resembled the cell area for each slice and background signals were removed using the provided algorithm of Fiji. The cell area of each slice was calculated by using a custom macro. The volume and mean cell area were calculated.

2.13. Mass spectrometry

2.13.1.1. Sample preparation for proteome analysis. For proteome analysis the samples were prepared by dissolving in 100 μl 1 % *w/v* sodium deoxycholate (SDC) in 0.1 M triethylammonium bicarbonate buffer (TEAB) and incubated for 10 min at 95 °C for cell lysis. Samples were sonicated for 5 s at an energy of 30 % to destroy interfering DNA.

Tryptic digestion was performed for 50 μg protein, using the single-pot, solid-phase-enhanced sample preparation (SP3) protocol, as described by [34]. Eluted peptides were dried in a Savant SpeedVac vacuum concentrator (Thermo Fisher Scientific, Waltham, USA) and stored at 20 °C until further use. Directly prior to measurement, dried peptides were resolved in 0.1 % formic acid (FA) in water (MS grade) to a final concentration of 1 μg/μl. In total, 1 μg was subjected to mass spectrometric analysis.

2.13.1.2. LC–MS/MS parameters. Liquid chromatography–tandem mass spectrometry measurements (LC–MS/MS) were performed on a quadrupole-ion-trap-orbitrap mass spectrometer (Orbitrap Fusion, Thermo Fisher). Chromatographic separation of peptides was achieved with a two-buffer system (buffer A: 0.1 % FA in H_2O (MS grade); buffer B: 0.1 % FA in acetonitrile (ACN, MS grade)). The samples were desalted and purified by loading onto a peptide trap column (180 μm × 20 mm, 100 Å pore size, 5 μm particle size, ACQUITY UPLC M-Class Symmetry C18, Waters), followed by a 25 cm C18 reversed-phase column (75 μm × 200 mm, 130 Å pore size, 1.7 μm particle size, nanoEase *M/Z* Peptide BEH C18, Waters) on an UPLC system. Peptides were separated using an 80 min gradient with trapping for 5 min at a flow rate of 5 μl/min followed by a linear increasing ACN concentration from 2 % to 30 % ACN in 65 min at a flow rate of 0.3 μl/min. Eluting peptides were ionized using a nano-electrospray ionization source (nano-ESI) with a spray voltage of 1800 V, transferred into the MS, and analyzed in data dependent acquisition (DDA) mode. For each MS1 scan, ions were accumulated for a maximum of 120 milliseconds or until a charge density of 2×10^5 ions (AGC Target) was reached. Fourier-transformation-based mass analysis of the data from the orbitrap mass analyzer was performed by covering a mass range of *m/z* 400–1300 with a resolution of 120,000 at m/z 200. Peptides with charge states between +2 to +5 above an intensity threshold of 1000 were isolated within an isolation window of *m/z* 1.6 in Top Speed mode for 3 s from each precursor scan and fragmented with a normalized collision energy of 30 %, using higher energy collisional dissociation (HCD). MS2 scanning was performed, using an ion trap mass analyzer at a rapid scan rate, with the first mass set to m/z 120 and accumulated for 60 ms or to an AGC target of 1×10^4. Already fragmented peptides were excluded for 30 s.

2.13.1.3. Raw data processing. LC-MS/MS data were searched with the SEQUEST algorithm integrated into the Proteome Discoverer software (v2.4.1.15, Thermo Fisher Scientific) against a reviewed human Swissprot database, obtained in December 2021, containing 20,340 entries. Carbamidomethylation was set as a fixed modification for cysteine residues. The oxidation of methionine was allowed as a variable modification as well as acetylation of the N-terminus and methionine loss. A maximum number of two missing tryptic cleavages was set. Peptides between six and 144 amino acids were considered. A strict cutoff (FDR < 0.01) was set for peptide and protein identification. Quantification was performed using Minora Algorithm, implemented in Proteome Discoverer v2.4. Obtained protein abundances were log2-transformed prior to statistical analysis and column mean normalized. For statistical analysis we considered 3530 proteins, which were detected in at least one condition with at least two biological replicates. Significant regulation was considered for proteins with log2(FC) $> \pm 1.5$ and a *p*-value <0.05. GO pathways enrichment was performed with String pathways analysis with a log2 ratio > 0.58, $p < 0.05$.

2.14. Data analysis

The statistical analysis was performed with GraphPad Prism version 8 (GraphPad Software, Inc.). Values are expressed as mean ± SEM. Group differences were analyzed by using two-way ANOVA with Tukey's multiple comparisons test for the data obtained in mice and one-way ANOVA with Holm-Sidak's or Tukey's multiple comparisons test for the data obtained in hiPSC-CMs. A value of $p < 0.05$ was considered statistically significant.

3. Results

3.1. Sac/Val improves cardiac function and attenuates pathological remodeling and hypertrophy after TAC

Echocardiographic measurements of TAC mice showed a continuous and significant decrease in cardiac systolic function parameters such as left ventricular (LV) ejection fraction (EF), cardiac output (CO), and stroke volume (SV) starting from day 14 after surgery compared to sham animals (Fig. 1A-C). In line with this, LV mass-to-body weight ratio (LVM/BW), LV end-diastolic anterior and posterior wall thicknesses (LVEDAW and LVEDPW, respectively), LV end-systolic diameter (LVESD), end-systolic volume (ESV), and LVM increased over time in TAC mice (Fig. 1D-F, H and Suppl. Fig. 1A, D). In contrast, no difference in LV end-diastolic diameter (LVEDD), end-diastolic volume (EDV), and body weight were observed over time between TAC and sham animals (Fig. 1G and Suppl. Fig. 1B, C). The administration of Sac/Val significantly improved cardiac function by decelerating the decrease in EF, CO, and SV and a smaller increase in LVEDPW in TAC animals from day 35 after surgery, i.e. after 21 days of treatment. Sac/Val treatment did not affect any parameter in the sham-treated mice. Thus, TAC mice showed LV hypertrophy and reduced cardiac systolic function, which was partially attenuated by the administration of Sac/Val.

3.2. Sac/Val partially normalizes some of TAC-induced changes in gene expression related to processes of heart failure

To further examine the disease state of TAC mice and the influence of Sac/Val on HF markers, changes in counts of mRNAs commonly associated with cardiac hypertrophy, fetal gene program, fibrosis, and Ca^{2+} handling were evaluated using the NanoString's nCounter® Elements technology (Table 1). While counts of mRNAs associated with hypertrophy (*Fhl1* and *Rcan1*) were higher, the counts of mRNAs associated with Ca^{2+} handling (*Atp2a2 and Pln*) were lower after TAC. In addition, counts of mRNAs associated with the reactivation of the fetal gene program (*Nppa, Nppb* and *Myh7*) as well as fibrosis (*Col1a1*, *Col3a1 and Postn*) were higher in TAC than in sham mice. The impact of Sac/Val administration on gene regulation of HF-associated markers was not entirely clear. Sac/Val administration partially normalized the expression of many factors of various biological processes such as *Rcan1*, *Myh7*, *Nppb*, *Atp2a2*, *Col1a1* and *Col3a1* compared to the TAC/vehicle group. Unexpectedly, Sac/Val altered the expression of some genes in TAC mice (*Fhl1*, *Nppa* and *Postn*) and sham mice *(Myh7* and *Nppa*).

3.3. Sac/Val attenuates TAC-induced fibrosis and hypertrophy

In addition to the Nanostring analyses of fibrosis and hypertrophy markers, corresponding staining was also performed in cardiac tissue. Consistent with a higher expression of *Col1a1* and *Col3a1* after TAC, sirius red staining showed a significant increase in collagen deposition, which in turn was markedly reduced by Sac/Val (Fig. 2A, B). Similarly, TAC induced a significant increase in cross sectional area (CSA) measured by dystrophin staining of heart tissue, indicating cardiomyocyte hypertrophy (Fig. 2C, D). Administration of Sac/Val significantly reduced cardiomyocyte hypertrophy in TAC mice.

3.4. Sac/Val does not impact on the expression of ALP markers

In order to investigate the effect of Sac/Val on the regulation of the ALP in HF mice, several markers involved in distinct stages of the ALP were determined on transcript level by RT-qPCR and on protein level by Western blot. The levels of beclin-1, which is involved in the phagophore structure initiation [19], did not significantly differ between the four investigated groups neither at transcript nor at protein level despite a tendency towards lower level in Sac/Val-treated TAC mice (Fig. 3A, B and Suppl. Fig. 2A). Next, we evaluated the microtubule-associated protein 1 light chain 3 beta (hereafter referred to as LC3), which exists at protein level in a soluble form termed LC3-I and in a lipidated form referred to as LC3-II, of which LC3-II is incorporated into the autophagosomal membrane and is involved in autophagosome formation and maturation, shuttling and fusion with the lysosomes [19]. The transcript and protein levels did not differ between the groups (Fig. 3A, C, D and Suppl. Fig. 2B). Whereas the expression of p62/sequestosome-1, which acts as a shuttle protein that binds ubiquitinated proteins and LC3-II and directs ALP-mediated degradation of ubiquitinated proteins [35], was significantly accumulated on transcriptional level, the protein level was not significantly altered, but tended to be higher in TAC/vehicle mice (Fig. 3A, E and Suppl. Fig. 2C). Sac/Val treatment had no significant effect on the p62/sequestosome-1 transcript and protein levels in sham and TAC mice. Furthermore, the evaluation of Rab-7, a small GTPase, which is important for membrane trafficking and autophagosome-lysosome fusion [36], revealed no alteration on mRNA level, whereas protein levels were lower after TAC intervention (Fig. 3A, F and Suppl. Fig. 2D). Administration of Sac/Val had no effect on the Rab-7 transcript and protein levels in sham and TAC mice. Finally, the mRNA level of the lysosomal-associated membrane protein-2 (LAMP-2) was higher, while the protein level did not differ in TAC/vehicle mice (Fig. 3A, G and Suppl. Fig. 2E). Similar to p62/sequestosome-1 and Rab-7, Sac/Val treatment had no effect on the LAMP-2 transcript and protein levels in sham and TAC mice.

3.5. Sac/Val reduces the TAC-induced increase in proteasome activity

Since accumulation of (poly)ubiquitinated proteins and altered proteasome activities have been reported in cardiac hypertrophy and HF [21–27], we determined the steady-state levels of (poly)ubiquitinated proteins by Western blot and measured the chymotrypsin-like activity of the 20S proteasome by using a synthetic fluorogenic substrate in heart tissue of TAC and sham mice with or without Sac/Val treatment. The steady-state levels of (poly)ubiquitinated proteins did not differ between the groups (Fig. 4A). In contrast, the chymotrypsin-like activity was ~2-fold higher in TAC than in sham mice, and Sac/Val administration significantly reduced the TAC-induced chymotrypsin-like activity to baseline level (Fig. 4B). Correlation analyses revealed a negative correlation between cardiac function (determined by the EF) and proteasome activity (determined by the chymotrypsin-like activity) and a positive correlation between the degree of cardiac hypertrophy (determined by the LVM/BW) and proteasome activity (Fig. 4C, D).

3.6. Sac alone or in combination with Val, but not Val alone prevents the hypertrophic gene program in hiPSC-CMs

We then wanted to decipher the mechanisms of the individual components of Sac/Val in more detail in a model of cellular hypertrophy in hiPSC-CMs. To induce cellular hypertrophy hiPSC-CMs were treated with 100 nM endothelin-1 (ET1), which was recently shown to induce a robust hypertrophic response in hiPSC-CMs [37]. To evaluate the impact of the individual active components of LCZ696, Sac and Val, hiPSC-CMs were treated with 40 μM Sac (in this case the active metabolite of the prodrug sacubitril, sacubitrilat, was used) or 13 μM Val or both 40 μM Sac + 13 μM Val (see experimental setup in Suppl. Fig. 3). The concentrations of Sac and Val were chosen according to plasma concentrations obtained in humans after treatment with 200 mg LCZ696 twice daily [10,38,39]. ET1 significantly increased mean cell area indicating cellular hypertrophy, which was normalized by all preventive treatments (Fig. 5A, B). In addition, ET1 caused a robust change in counts of mRNAs commonly associated with hypertrophy (*FHL1* and *RCAN1*), reactivation of the fetal gene program (*NPPB* and *MYH7*) or fibrosis (*CTGF*, *ACTA2* and *FN1*; Table 2). The changes in *MYH6/MYH7* expression mimicked the classical isoform switch between α- and β-myosin heavy chains. Only Sac and Sac/Val partially normalized these changes. The combination of Sac/Val was slightly superior to Sac alone

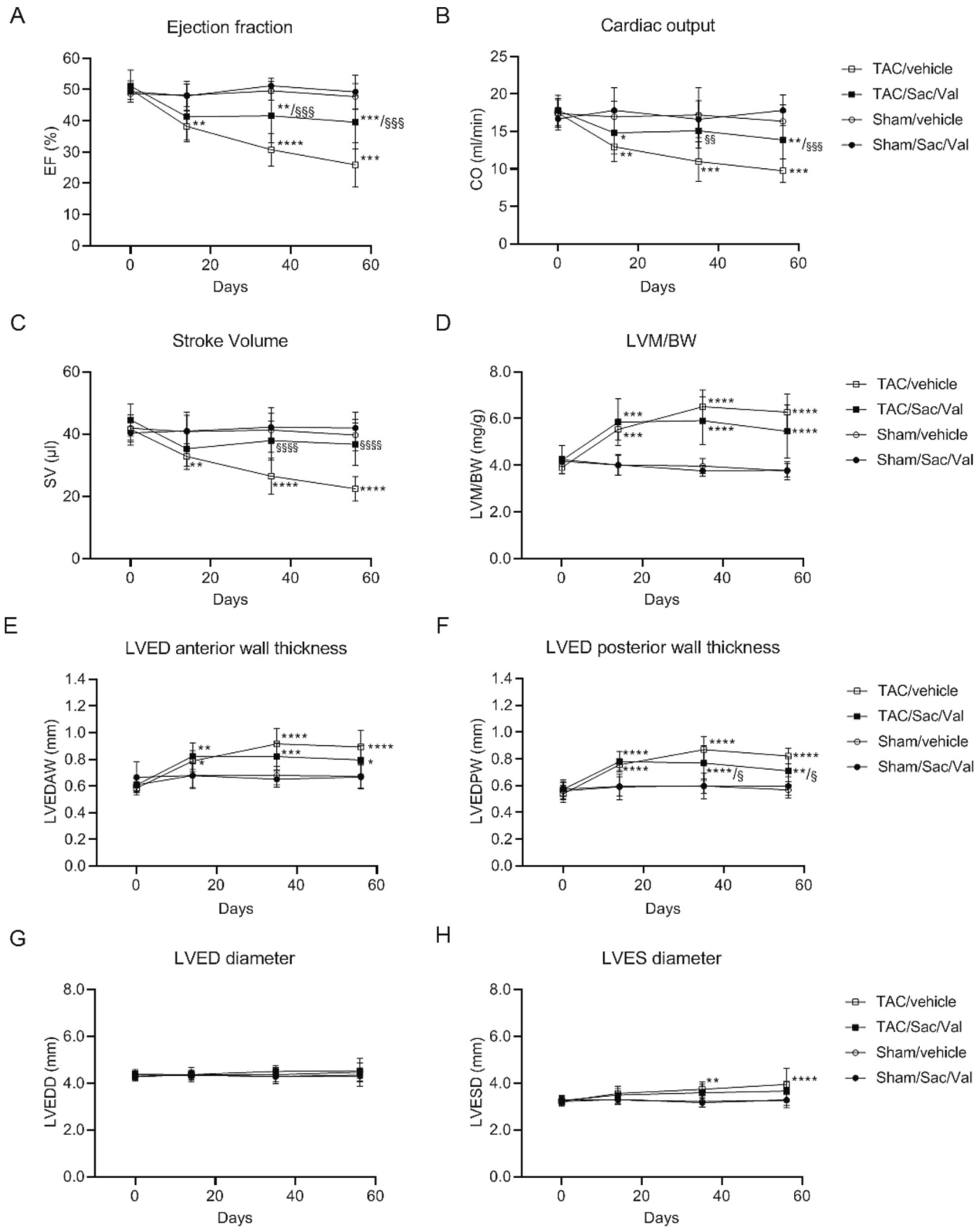

Fig. 1. Evaluation of functional and morphological heart parameters in TAC and sham mice with and without Sac/Val treatment. Scatter plots show the difference in (A) ejection fraction (EF), (B) cardiac output (CO), (C) stroke volume (SV), (D) left ventricular (LV) mass/body weight (LVM/BW), (E) LV end-diastolic (ED) anterior wall thickness (LVEDAW), (F) LVED posterior wall thickness (LVEDPW), (G) LVED diameter (LVEDD), and (H) LV end-systolic (ES) diameter (LVESD) of TAC and sham mice with and without Sac/Val treatment. The individual groups are represented by specific symbols. Data are presented as mean ± SEM with *$p < 0.05$, **$p < 0.01$, ***$p < 0.001$ and ****$p < 0.0001$ vs. corresponding sham group, and $^{§}p < 0.05$, $^{§§}p < 0.01$, $^{§§§}p < 0.001$ and $^{§§§§}p < 0.0001$ vs. TAC/vehicle group, two-way ANOVA. N = 10.

Table 1
Gene expression analysis in sham and TAC mice.

Gene acronym	Gene name	Sham/ Sac/Val	TAC/ vehicle	TAC/ Sac/Val
Markers of hypertrophy				
Fhl1	Four and half LIM domains 1	1.03	1.87	2.09
Fhl2	Four and half LIM domains 2	0.86	0.98	0.88
Rcan1	Regulator of calcineurin 1	0.75	1.56	1.39
Markers of fetal gene program				
Actc1	Actin alpha cardiac muscle 1	0.94	1.00	0.95
Myh6	Myosin heavy chain 6	1.07	0.89	0.91
Myh7	Myosin heavy chain 7	2.60	16.20	9.51
Nppa	Natriuretic peptide A	1.97	9.73	10.81
Nppb	Natriuretic peptide B	0.68	3.03	2.61
Markers of Ca^{2+} handling				
Atp2a2	ATPase, Ca++ transporting, cardiac muscle, slow twitch 2	1.15	0.77	0.92
Pln	Phospholamban	1.12	0.77	0.78
Ryr2	Ryanodine receptor 2	1.11	0.85	0.81
Markers of fibrosis				
Col1a1	Collagen, type I, alpha1	0.91	1.73	1.32
Col3a1	Collagen, type III, alpha 1	0.85	1.40	1.12
Nfkb1	Nuclear factor kappa B, subunit 1	0.96	0.90	1.07
Fibroblast-specific marker				
S100a4	S100 calcium binding protein A4	1.00	1.09	1.16
Postn	Periostin, osteoblast specific factor	0.87	3.16	3.35

Gene expression analysis of indicated genes was performed in sham and TAC mice (n = 3) with and without sacubitril/valsartan (Sac/Val) treatment with the NanoString nCounter® Elements technology. Data were normalized to housekeeping genes and are expressed as fold-change over sham/vehicle.

while Val alone showed no effect. This emphasizes the importance of Sac in preventing ET1-induced hypertrophic gene program in this model.

Further, proteomic analysis by mass spectrometry (MS) was performed. Volcano plots depict 240 (197 higher, 43 lower) dysregulated proteins in ET1-treated samples vs. control (Fig. 6A). Significantly increased levels of a number of proteins which are associated with cellular hypertrophy and cytoskeletal modulations (ACTA1, ACTB, ACTN1, ACTN2, ACTN4, CRYAB, FLNA, FLNB, FLNC, FHL1, FHL2, MAP1B, NPPA, TNNI3, TNNT2, VIM) were uncovered in the ET1-treated hiPSC-CMs compared to control. The application of Sac and Sac + Val successfully prevented some of these increases (FLNA, FLNB, FHL1, MAP1B, TNNI3, VIM for Sac and ACTA1, ACTB, CRYAB, FHL1, FHL2, MAP1B, TNNI3 for Sac + Val, respectively), while Val alone failed to do so. Overall, the combination of Sac + Val resulted in more proteomic changes than the individual compounds (83 higher, 107 lower for Sac + Val compared to 44 higher, 40 lower for Sac and 41 higher, 66 lower for Val, respectively). GO pathway analysis of MS revealed that ET1-treated samples were enriched in proteins associated with cytoskeletal processes and remodeling (Fig. 6B). Only in the two groups that received Sac, cytoskeletal and sarcomeric processes were modified compared to the ET1 only group, while Val failed to cause this effect. Interestingly, proteomic changes due to Val treatment were mostly associated with mitochondrial aberrations.

3.7. ET1-induced increase in proteasome activity is not significantly affected by the treatments in hiPSC-CMs

Since Sac/Val administration significantly reduced the TAC-induced chymotrypsin-like activity to normal level in mice (Fig. 4B), we also measured the chymotrypsin-like activity in the treated hiPSC-CMs. Similar to TAC in mice, ET1 treatment resulted in a 2-fold induction of the chymotrypsin-like activity in hiPSC-CMs ($p = 0.011$ vs. control only with unpaired Student's *t*-test; Fig. 7A). This ET1-induced increase in chymotrypsin-like activity was not significantly affected by the different treatments. Unexpectedly, but again similar to TAC in mice, ET1 treatment did not result in higher steady-state levels of (poly) ubiquitinated proteins (Fig. 7B). However, treatment with Sac/Val significantly reduced the steady-state levels of (poly)ubiquitinated proteins.

4. Discussion

In the present study we investigated whether the ARNI Sac/Val influenced the cardiomyopathic phenotype and the two proteolytic systems namely UPS and ALP in a mouse model of TAC and in a human cellular model of cardiac hypertrophy. The major findings of the present study were: (1) Sac/Val improved cardiac function and attenuated hypertrophy and fibrosis after TAC in mice, (2) Sac/Val did not impact on the ALP in mice, (3) Sac/Val reduced the TAC-induced increase in

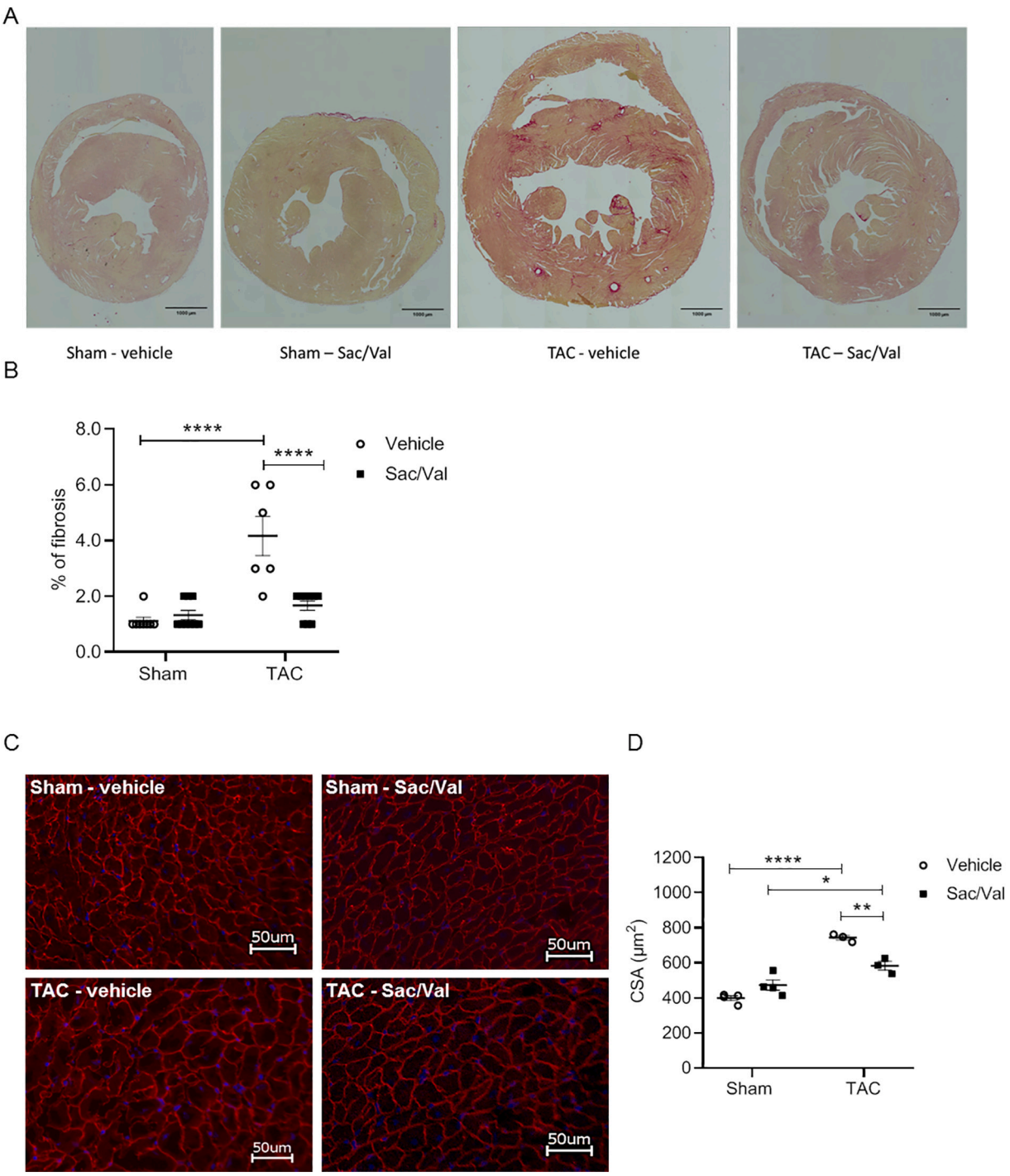

Fig. 2. Analyses of various markers associated with fibrosis and hypertrophy in TAC and sham mice with and without Sac/Val treatment. (A) Representative images of Sirius red staining. (B) Quantitative analysis of cardiac fibrosis using Sirius red staining (N = 6–9). (C) Representative images of dystrophin-stained heart sections. Magnification 20× with dystrophin in red and DAPI (= nuclei) in blue. (D) Quantitative analysis of the cross-sectional area (CSA) of individual cardiomyocytes (n = 3–4). Data are presented as mean ± SEM with *p < 0.05, **p < 0.01 and ****p < 0.0001 vs. indicated group, two-way ANOVA with Tukey's multiple comparisons test. (For interpretation of the references to colour in this figure legend, the reader is referred to the web version of this article.)

proteasome activity to normal level in mice, (4) Sac and Sac/Val, but not Val alone prevented ET1-induced hypertrophic gene program and most of the proteomic changes in hiPSC-CMs.

Overall, we confirmed the beneficial effects of Sac/Val on cardiac function, hypertrophy and fibrosis in our mouse model of pressure overload, but due to our study design we could not distinguish whether these beneficial effects originate from neprilysin inhibition or angiotension receptor blockade or both. However, our data obtained in hiPSC-CMs suggest a superiority of Sac over Val. Our findings aligned with a previous study by Burke et al. who demonstrated in a mouse model of pressure overload-induced HF that Sac/Val was more effective than Val alone in reducing cardiac hypertrophy, systolic dysfunction, and cardiac fibrosis [40]. Additional *in vitro* studies in human cardiac fibroblasts revealed that the beneficial effects on cardiac fibrosis were at least partially due to the sacubitrilat component of Sac/Val functioning by preventing suppression of protein kinase G signaling. In streptozotocin-

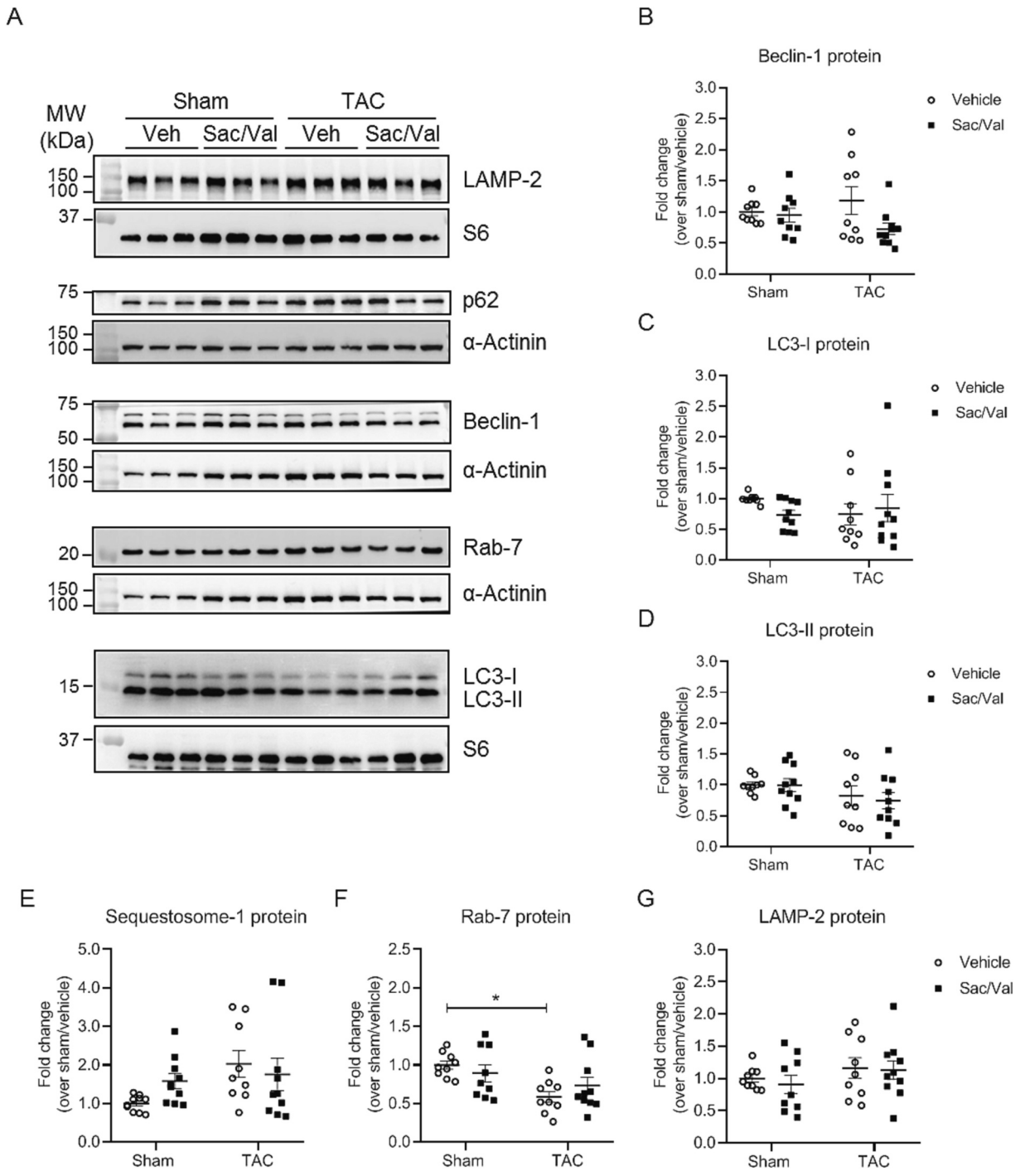

Fig. 3. Evaluation of the ALP at protein level in TAC and sham mice with and without Sac/Val treatment. (A) Representative Western blots of indicated proteins. A–Actinin and S6 ribosomal protein were used as loading controls. Quantification of (B) Beclin-1, (C) LC3-I, (D) LC3-II, (E) p62/sequestosome-1, (F) Rab-7, and (G) LAMP-2 protein levels normalized to α–actinin or S6 ribosomal protein and related to sham/vehicle. Data are presented as mean ± SEM with *p < 0.05 vs. indicated group, two-way ANOVA with Tukey's multiple comparisons test. N = 9–10.

induced diabetic mice with HF with reduced LVEF, Sac/Val and Val alone have been shown to reduce myocardial hypertrophy to a similar degree, while Sac/Val was superior over Val alone in terms of lowering fibrosis and improving systolic function [41]. Summarizing all studies suggests that the favorable effects on cardiac function and fibrosis originate from Sac or at least that there is an additional effect from neprilysin inhibition compared with angiotension receptor blocker alone. With regard to cardiac hypertrophy the data are not yet conclusive, since at least in one study Sac/Val and Val alone have been shown to reduce hypertrophy to a similar degree suggesting that angiotensin receptor blockade is primarily responsible for the anti-hypertrophic effect, whereas in the other models Sac/Val or Sac alone was superior to Val alone.

The effect of ARNI on UPS and ALP has not been examined yet intensively and was thus a new subject of our investigations. Alterations of the autophagic flux and dysregulated expression of ALP key marker have been observed in a wide range of cardiac diseases such as desmin-related cardiomyopathy [42–44], dilated cardiomyopathy [44–46] and

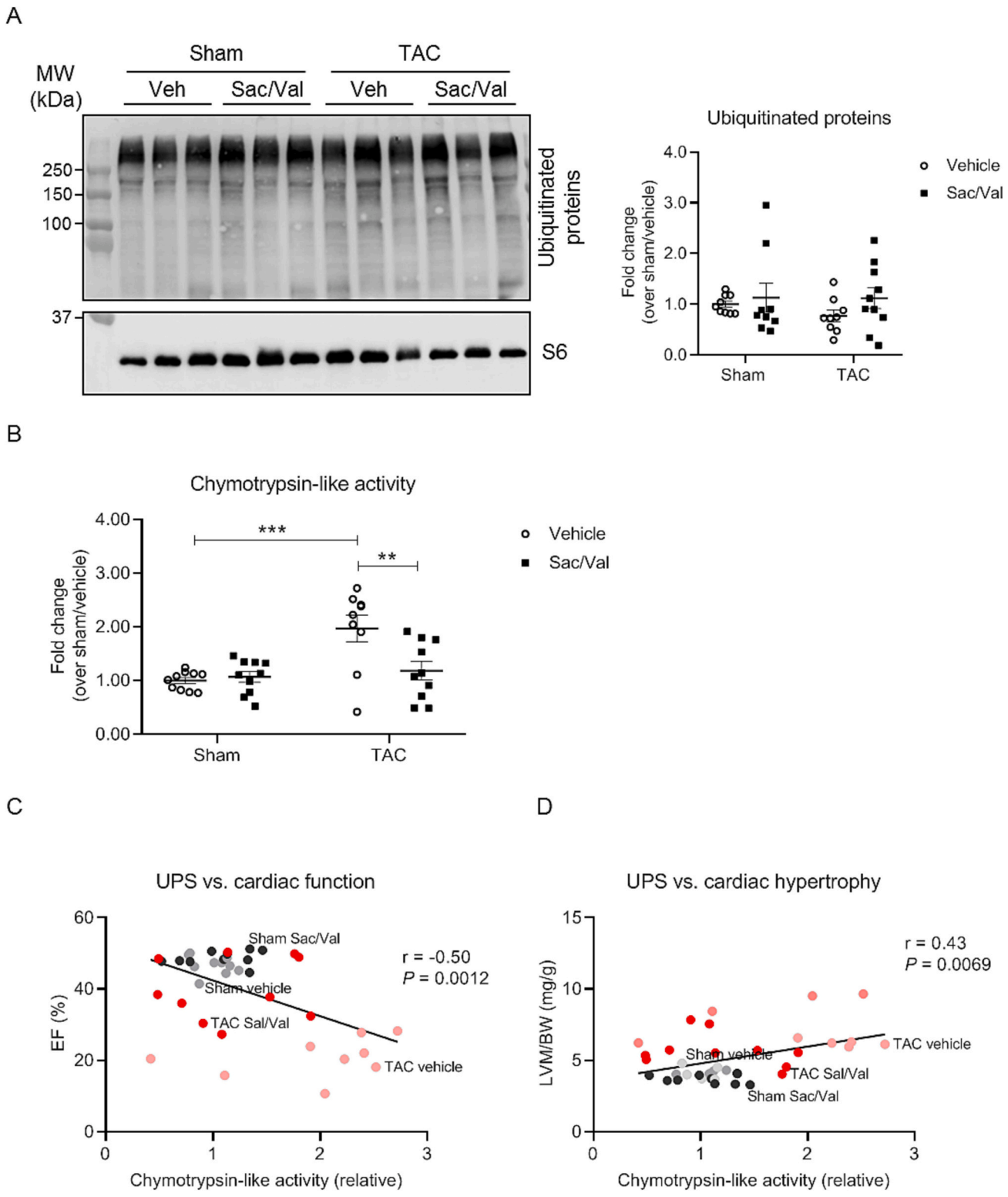

Fig. 4. Evaluation of the UPS in TAC and sham mice with and without Sac/Val treatment. (A) Representative Western blot and quantification of the steady-state levels of (poly)ubiquitinated proteins normalized to S6 ribosomal protein and related to WT. (B) 20S chymotrypsin-like activity was measured by using a specific fluorogenic substrate. (C) Correlation between the UPS activity (represented by the chymotrypsin-like activity) and cardiac function (represented by the ejection fraction (EF)). (D) Correlation between the UPS activity (represented by the chymotrypsin-like activity) and hypertrophy (represented by the left ventricular mass/body weight (LVM/BW)). Analyses of Spearman correlation factor (r) were performed with indicated *p* values. Data points in (C) and (D) are shown in grey for sham vehicle, in black for sham Sac/Val, in light red for TAC vehicle and in red for TAC Sac/Val, respectively. Data for (A) and (B) are presented as mean ± SEM with $^{**}p < 0.01$ and $^{***}p < 0.001$ vs. indicated group, two-way ANOVA with Tukey's multiple comparisons test. N = 9–10. (For interpretation of the references to colour in this figure legend, the reader is referred to the web version of this article.)

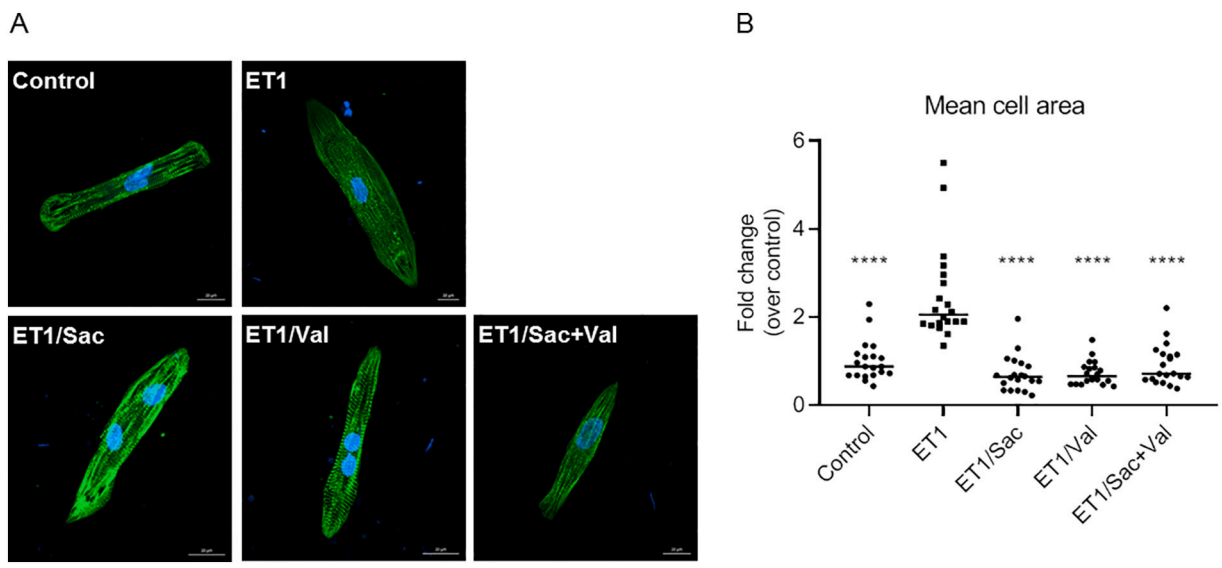

Fig. 5. Evaluation of cellular hypertrophy in 2D hiPSC-CMs with chronic intervention with Sac, Val or Sac combined with Val. Human induced pluripotent stem cell-derived cardiomyocytes (hiPSC-CMs) were treated for 72 h with 0.08 % DMSO (control), 100 nM endothelin-1 (ET1) + 0.08 % DMSO, 100 nM ET1 + 40 μM Sac, 100 nM ET1 + 13 μM Val, or 100 nM ET1 + 40 μM Sac + 13 μM Val. (A) Representative immunofluorescent images of hiPSC-CMs stained with an antibody specific for α-actinin and Hoechst33342 for visualization of the nuclei. Scale bar = 20 μm. (B) Mean cell area was analyzed after 72 h via immunofluorescence imaging and subsequent quantification. Data are presented as mean ± SEM and are expressed as fold-change over control with ****$p < 0.0001$ vs. ET1, one-way ANOVA with Holm-Sidak's multiple comparisons test. N = 20.

Table 2
Gene expression analysis in endothelin-1-treated 2D hiPSC-CMs.

Gene acronym	Gene name	ET1	ET1/Sac	ET1/Sac+Val	ET1/Val
Markers of hypertrophy					
FHL1	Four and half LIM domains 1	2.14	1.23	1.12	2.14
FHL2	Four and half LIM domains 2	0.54	0.93	0.95	0.95
RCAN1	Regulator of calcineurin 1	1.85	1.26	1.02	2.13
Markers of fetal gene program					
ACTA1	Actin alpha 1, skeletal muscle	3.21	2.24	2.00	3.92
MYH6	Myosin heavy chain 6	0.45	0.91	0.78	0.64
MYH7	Myosin heavy chain 7	15.60	5.67	3.81	13.82
NPPA	Natriuretic peptide A	1.84	1.54	1.28	2.04
NPPB	Natriuretic peptide B	8.58	3.94	2.47	8.46
Markers of Ca^{2+} handling					
PLN	Phospholamban	1.42	1.15	0.87	1.32
Markers of fibrosis					
CTGF	Connective tissue growth factor	2.73	1.43	1.11	1.72
ACTA2	Actin alpha 2, smooth muscle	2.08	1.20	0.99	1.41
FN1	Fibronectin 1	1.71	0.77	0.80	1.13
Fibroblast-specific marker					
S100A4	S100 calcium binding protein A4	1.62	0.57	0.43	0.93

Gene expression analysis of indicated genes was performed in hiPSC-CMs treated for 72 h with 0.08 % DMSO (control), 100 nM endothelin 1 (ET1) + 0.08 % DMSO, 100 nM ET1 + 40 μM Sac, 100 nM ET1 + 13 μM Val, or 100 nM ET1 + 40 μM Sac + 13 μM Val with the NanoString nCounter® Elements technology. Data were normalized to housekeeping genes and are expressed as fold-change over DMSO control (pools with n = 3 per group).

hypertrophic cardiomyopathy with reduced EF [26,47]. The role of the ALP in the development of cardiac hypertrophy and its progression to HF has been discussed controversially [28,48]. The impact of TAC, used as a model of pressure overload, on the ALP has as well led to controversial results. One study showed that autophagic activity reached a peak at 48 h following TAC and remained significantly elevated for at least 3 weeks [28]. Another study reported that autophagic flux was transiently activated after TAC, peaking within 3 to 12 h, but suppressed after 7 days

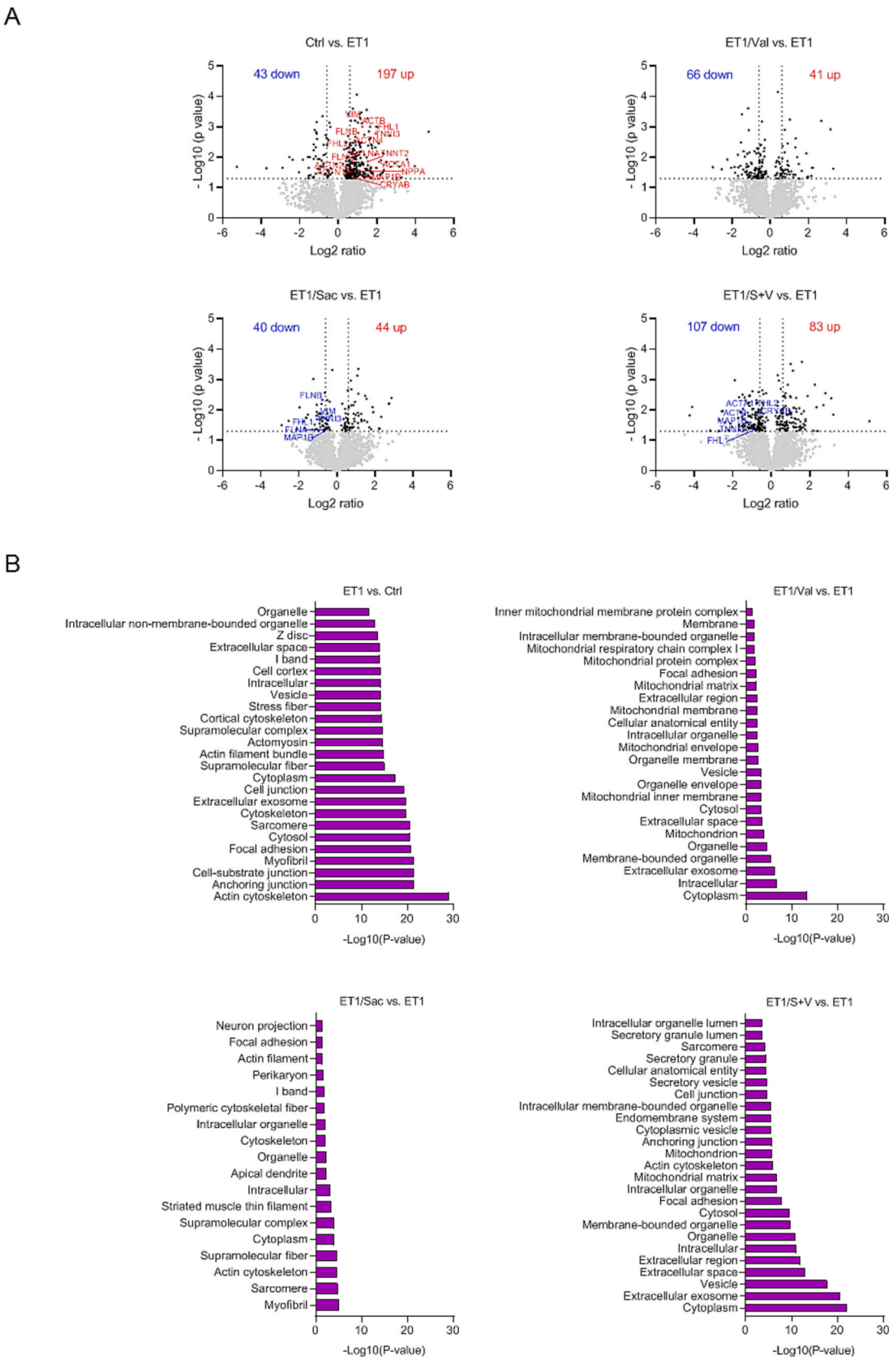

Fig. 6. Evaluation of proteomic changes in 2D hiPSC-CMs with chronic intervention with Sac, Val or Sac combined with Val. Human induced pluripotent stem cell-derived cardiomyocytes (hiPSC-CMs) treated for 72 h with 0.08 % DMSO (control), 100 nM endothelin-1 (ET1) + 0.08 % DMSO, 100 nM ET1 + 40 μM Sac, 100 nM ET1 + 13 μM Val, or 100 nM ET1 + 40 μM Sac + 13 μM Val were analyzed with differential quantitative proteomics. N = 3 per group. (A) Volcano plots show the -Log10 (*p*-value) vs. the magnitude of change (log2 ratio) of protein levels in the respectively compared groups; light grey dots indicate $p > 0.05$ and dark grey dots $p < 0.05$. (B) Major string GO pathways enrichment in the respectively compared groups; log2 ratio > 0.58, $p < 0.05$.

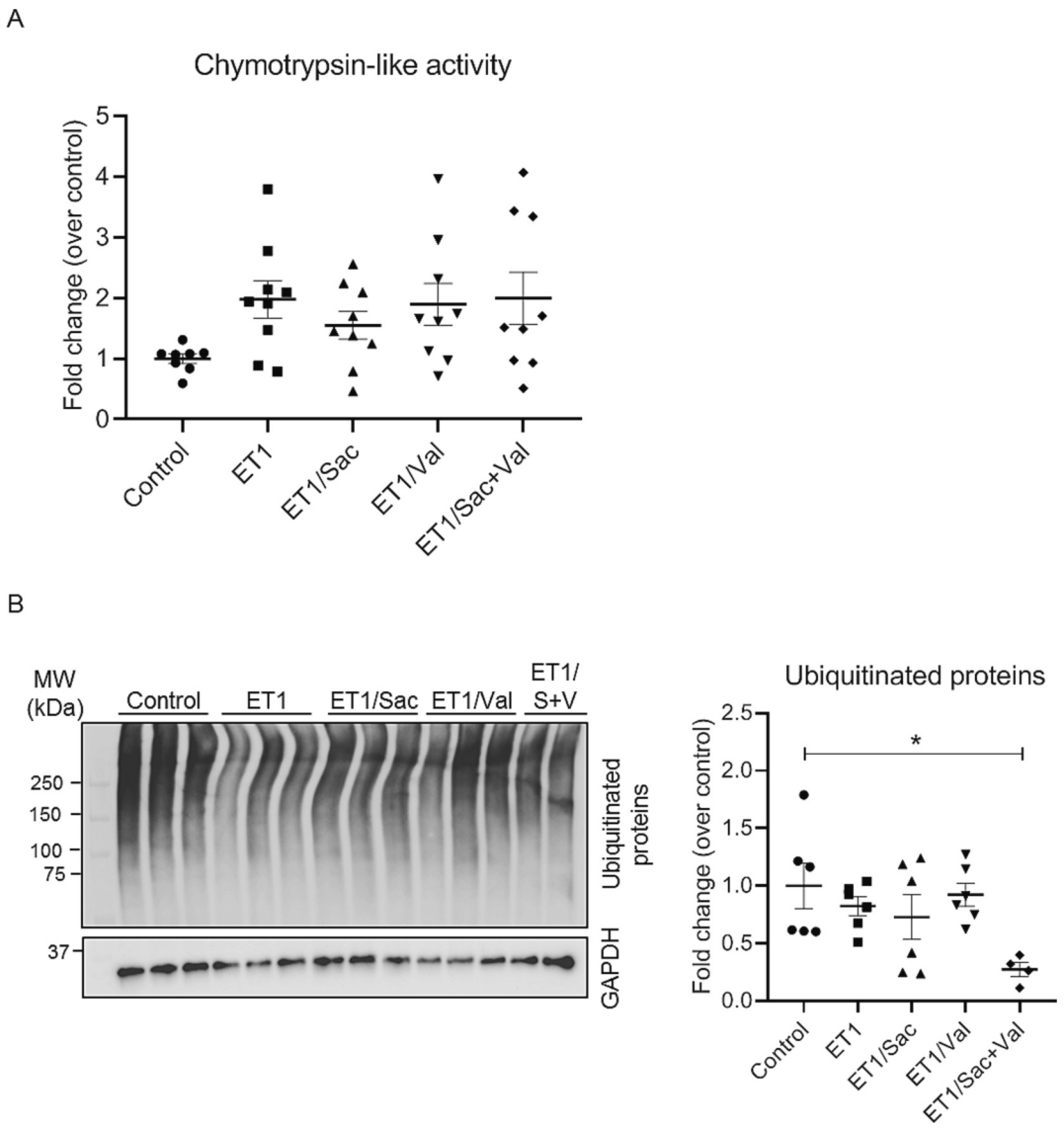

Fig. 7. Evaluation of the UPS in 2D hiPSC-CMs with chronic intervention with Sac, Val or Sac combined with Val. Human induced pluripotent stem cell-derived cardiomyocytes (hiPSC-CMs) were treated for 72 h with 0.08 % DMSO (control), 100 nM endothelin-1 (ET1) + 0.08 % DMSO, 100 nM ET1 + 40 μM Sac, 100 nM ET1 + 13 μM Val, or 100 nM ET1 + 40 μM Sac + 13 μM Val. (A) 20S chymotrypsin-like activity was measured by using a specific fluorogenic substrate. N = 8–9. (B) Representative Western blot and quantification of the steady-state levels of (poly)ubiquitinated proteins normalized to GAPDH and related to control. N = 4–6. Data are presented as mean ± SEM with *p < 0.05 vs. indicated group, one-way ANOVA with Tukey's multiple comparisons test.

[49]. In a more recent study using a mouse model of HF that combines moderate TAC and distal LAD ligation (myocardial infarction [MI]), a decreased autophagic flux was noted 6 weeks after TAC-MI [50]. In our present study we did not observe major alterations of the ALP 8 weeks after TAC, only p62/sequestosome-1 protein levels tended to be higher and Rab-7 protein levels were lower after TAC intervention, respectively. More importantly, administration of Sac/Val had no further effect on the ALP, only beclin-1 protein levels tended to be lower after Sac/Val administration in TAC mice. Interestingly, in a rat model of hyperthyroidism-induced cardiac hypertrophy, Sac/Val and Val alone normalized the levels of ALP markers, with consistently stronger effects of Sac/Val over Val alone [51].

Perturbations in the degradation process of the UPS have been as well widely reported in cardiac diseases [16–18,20]. While a marked accumulation of (poly)ubiquitinated proteins has been shown as a common feature of cardiac disorders [21–23], higher or lower proteasome activities have been reported depending on the status of the cardiac disease [22–27]. Unexpectedly, we did not observe higher steady-state levels of (poly)ubiquitinated proteins in our present study, neither after TAC in mice nor after ET1 treatment in hiPSC-CMs. However, the chymotrypsin-like activity was elevated both after TAC in mice and after ET1 treatment in hiPSC-CMs. This is in line with other studies showing proteasome activation in mice and dogs after TAC [24,52]. Admittedly, an activated proteasome was not detected consistently and a study by Tsukamoto et al. reported depression of proteasome activities after TAC in mice [25]. The novelty of our study is that Sac/Val administration significantly reduced the TAC-induced chymotrypsin-like activity to baseline level in mice. To the best of our knowledge there is no other study that has examined the effect of Sac/Val on UPS function and the mechanism behind neprilysin inhibition and/or angiotensin receptor blockade and reduction of proteasome activity merits further investigation.

However, the ability of neprilysin inhibitors to increase the levels of natriuretic peptides brought cyclic guanosine monophosphate (cGMP)-dependent protein kinase (PKG) into focus as a potential target of Sac/Val. Increased circulating natriuretic peptides bind to the natriuretic

peptide receptor, which activates membrane guanylate cyclases to synthesize intracellular cGMP and ultimately activate PKG [53]. Different studies showed that activated PKG can increase the activity of the proteasome. In transgenic mice expressing a surrogate substrate (GFPdgn), activation of PKG by sildenafil, a phosphodiesterase 5 inhibitor raising cGMP by blocking its hydrolysis to GMP, increased myocardial proteasome activities and decreased myocardial GFPdgn protein levels [54]. Since no significant changes in proteasome subunit abundance were detected after sildenafil treatment in mouse hearts and cultured cardiomyocytes, the authors concluded that the altered proteasome abundance was unlikely the underlying mechanism, but rather posttranslational modifications to proteasome subunits, likely phosphorylation, may be the mechanism by which PKG activation modulates proteasomal function. Interestingly, activation of PKG by sildenafil showed no discernible effects on the two major ALP marker proteins LC3-II and p62/sequestosome-1 in the transgenic GFPdgn mouse hearts. Another study also demonstrated that agents that raise cGMP and activate PKG stimulate 26S proteasome activities by phosphorylation and intracellular proteolysis without affecting the ALP [55]. The induction of proteasome activities and protein turnover by cGMP and PKG seemed to be a general cellular response, since similar effects were observed in different kinds of cell types, e.g. in neuroblastoma cells, HEK293 cells and human fibroblasts. Furthermore, inhibiting phosphodiesterase 1, which hydrolyzes both cyclic adenosine monophosphate and cGMP, also increased the 26S proteasome activity in a $CryAB^{R120G}$-based mouse model of proteinopathy [56]. These studies demonstrated that PKG is an important regulator of proteasome-mediated proteolysis. In contrast to these studies, we observed a reduction of the proteasome activity after an assumed activation of PKG due to neprilysin inhibition by Sac. However, this reduction of proteasome activity had a beneficial, positive regulating impact by reducing a pathologically TAC-induced chymotrypsin-like activity back to baseline level. In addition, neprilysin inhibition may improve outcomes through mechanisms other than PKG signaling. For instance, Tam et al. examined the effects of Sac/Val in a chronic, moderate LV pressure overload model in WT mice and mice harboring mutations in the PKGI alpha isoform, the predominant PKG isoform in the heart. They showed that the PKGI alpha mutations did not diminish the beneficial effects of Sac/Val on cardiac hypertrophy and LV function suggesting that signaling other than natriuretic peptide-cGMP-PKG mediated the benefits of neprilysin inhibition [57].

Although our data suggest that the beneficial effects on cardiac hypertrophy, function, fibrosis, and UPS rely in particular on Sac, neprilysin inhibition is not an option for monotherapy. In addition to contributing to the breakdown of the cardioprotective counter-regulatory natriuretic peptides, neprilysin is also involved in the degradation of vasoconstrictors such as ET1 and angiotension II [58], a peptide known to mediate long-term adverse effects on the heart and blood vessels. Initial attempts to inhibit neprilysin using racecodotril or candoxatrilat were successful in promoting natriuresis and increasing urinary ANP excretion [59,60]. However, a study of chronic use (28 days) of the prodrug candoxatril, showing significantly increased ANP levels, did not produce a clinically relevant decrease in blood pressure [61], possibly due to reduced neprilysin-mediated ET1 and angiotensin II degradation. Thus, the inhibition of neprilysin alone is not sufficient to counterbalance the activation of the renin-angiotensin-aldosterone system in cardiovascular diseases (e.g. hypertension and HF) and a combination of angiotensin receptor blockade and neprilysin inhibition is needed to block the effect of the excess angiotensin II.

4.1. Limitations

We acknowledge several limitations in our study. First, we did not observe higher steady-state levels of (poly)ubiquitinated proteins neither after TAC in mice nor after ET1 treatment in hiPSC-CMs. This was unexpected, since a marked accumulation of (poly)ubiquitinated proteins is a hallmark of cardiac disorders [21–23] and associated with either higher or lower proteasome activities [22–27]. Second, in contrast to the findings in mice, Sac, Val or the combination of both did not significantly reduce the ET1-induced chymotrypsin-like activity in hiPSC-CMs, though a tendency was observed with Sac. Beside the high variability of measurements in hiPSC-CMs, which are, by definition, enriched in CMs (about 82 % in our study vs. generally assumed 30 % in mouse hearts), we cannot exclude that some of the beneficial effects of Sac/Val in mice involve other cell types than cardiomyocytes, such as endothelial, smooth muscle or fibroblast cells. Indeed, there is some evidence that the UPS may be considered as a modulator of endothelial function by interaction with pathways involved in endothelial cell signaling, inflammation, and oxidative stress. It has been suggested that the UPS is modified by mediators (e.g. nitric oxide) and processes (e.g. oxidative stress) involved in the regulation of endothelial function and may itself modulate the expression and phosphorylation of endothelial nitric oxide synthase [62]. Interestingly, a recent study showed protective effects of Sac/Val against cardiac hypertrophy, fibrosis and inflammation by suppressing NF-κB signaling and NLRP3 inflammasome activation in mice after relief of pressure overload [63]. Third, due to our study design in mice and the fact that the data in hiPSC-CMs were not conclusive enough, we are not yet able to distinguish whether the positive-regulating effects on proteasome activity are attributed to Sac, Val or the combination of both and the association between neprilysin inhibition and/or angiotensin receptor blockade and reduction of proteasome activity remains elusive and needs further investigation.

5. Conclusion

Sac/Val normalized proteasome activity, improved cardiac function and reduced fibrosis and hypertrophy in TAC mice. Molecular analyses in hiPSC-CMs suggest that a major part of the beneficial effect of Sac/Val is derived from the Sac action rather than Val.

Supplementary data to this article can be found online at https://doi.org/10.1016/j.jmccpl.2023.100059.

Funding

This study was supported by the German Centre for Cardiovascular Research (DZHK; Grant B17-014) to SK and LC and the Leducq Foundation (20CVD01) to LC.

CRediT authorship contribution statement

Moritz Meyer-Jens: Data curation, Formal analysis, Investigation, Methodology, Writing – review & editing, Writing – original draft. **Kristin Wenzel:** Conceptualization, Data curation, Formal analysis, Investigation, Methodology, Writing – review & editing, Writing – original draft. **Karina Grube:** Conceptualization, Data curation, Formal analysis, Investigation, Methodology. **Julia Rüdebusch:** Conceptualization, Data curation, Formal analysis, Investigation. **Elisabeth Krämer:** Data curation, Investigation, Methodology. **Martin Bahls:** Conceptualization. **Kilian Müller:** Data curation, Formal analysis, Investigation. **Hannah Voß:** Data curation, Formal analysis, Investigation. **Hartmut Schlüter:** Data curation, Formal analysis, Methodology, Writing – review & editing. **Stephan B. Felix:** Conceptualization. **Lucie Carrier:** Conceptualization, Data curation, Formal analysis, Funding acquisition, Project administration, Writing – review & editing, Writing – original draft. **Stephanie Könemann:** Conceptualization, Data curation, Formal analysis, Funding acquisition, Project administration, Writing – original draft, Writing – review & editing. **Saskia Schlossarek:** Conceptualization, Data curation, Formal analysis, Investigation, Writing – original draft, Writing – review & editing.

Declaration of competing interest

The authors declare the following financial interests/personal

relationships which may be considered as potential competing interests: Karina Grube reports equipment, drugs, or supplies was provided by Novartis AG. Stephan B. Felix reports equipment, drugs, or supplies was provided by Novartis AG. Lucie Carrier reports financial support was provided by German Center for Cardiovascular Disease. Stephanie Könemann reports financial support was provided by German Center for Cardiovascular Disease. Lucie Carrier reports financial support was provided by Leducq Foundation. Stephanie Könemann reports a relationship with Novartis AG that includes: speaking and lecture fees. Stephanie Könemann reports a relationship with Daiichi Sankyo that includes: speaking and lecture fees. Stephanie Könemann reports a relationship with AstraZeneca that includes: speaking and lecture fees. Karina Grube reports a relationship with Cheplapharm Arzneimittel GmbH that includes: employment. Lucie Carrier reports a relationship with Dinaqor AG that includes: board membership. If there are other authors, they declare that they have no known competing financial interests or personal relationships that could have appeared to influence the work reported in this paper.

Data availability

The mass spectrometry proteomics data have been deposited to the ProteomeXchange Consortium via the PRIDE [64] partner repository with the dataset identifier PXD044170. Other data underlying this article will be shared on reasonable request to the corresponding authors.

Acknowledgement

Sac/Val administered to the mice was provided from Novartis AG (Basel, Switzerland).

The authors would like to thank Ines Urbaneck, Lisa Maletzki and Annika Reuser (Department of Internal Medicine B, Greifswald) for supporting the animal experiments. The authors gratefully acknowledge Birgit Klampe, Thomas Schulze and Grit Höppner (Institute of Experimental Pharmacology and Toxicology, Hamburg) for preparing various media for the culture of hiPSC-CMs.

References

[1] Sauer AJ, Cole R, Jensen BC, Pal J, Sharma N, Yehya A, et al. Practical guidance on the use of sacubitril/valsartan for heart failure. Heart Fail Rev 2019;24:167–76.
[2] Cruden NLM, Fox KAA, Ludlam CA, Johnston NR, Newby DE. Neutral endopeptidase inhibition augments vascular actions of bradykinin in patients treated with angiotensin-converting enzyme inhibition. Hypertension 2004;44:913–8.
[3] Rademaker MT, Charles CJ, Espiner EA, Nicholls MG, Richards AM, Kosoglou T. Neutral endopeptidase inhibition: augmented atrial and brain natriuretic peptide, haemodynamic and natriuretic responses in ovine heart failure. Clin Sci 1996;91:283–91.
[4] Wilkinson IB, McEniery CM, Bongaerts KH, MacCallum H, Webb DJ, Cockcroft JR. Adrenomedullin (ADM) in the human forearm vascular bed: effect of neutral endopeptidase inhibition and comparison with proadrenomedullin NH2-terminal 20 peptide (PAMP). Br J Clin Pharmacol 2001;52:159–64.
[5] Woods RL. Cardioprotective functions of atrial natriuretic peptide and B-type natriuretic peptide: a brief review. Clin Exp Pharmacol Physiol 2004;31:791–4.
[6] Maric C, Zheng W, Walther T. Interactions between angiotensin ll and atrial natriuretic peptide in renomedullary interstitial cells: the role of neutral endopeptidase. Nephron Physiol 2006;103:p149–56.
[7] Kuhn M. Molecular physiology of natriuretic peptide signalling. Basic Res Cardiol 2004;99:76–82.
[8] Solomon SD, Zile M, Pieske B, Voors A, Shah A, Kraigher-Krainer E, et al. The angiotensin receptor neprilysin inhibitor LCZ696 in heart failure with preserved ejection fraction: a phase 2 double-blind randomised controlled trial. Lancet 2012;380:1387–95.
[9] McMurray JJ, Packer M, Desai AS, Gong J, Lefkowitz MP, Rizkala AR, et al. Dual angiotensin receptor and neprilysin inhibition as an alternative to angiotensin-converting enzyme inhibition in patients with chronic systolic heart failure: rationale for and design of the Prospective comparison of ARNI with ACEI to Determine Impact on Global Mortality and morbidity in Heart Failure trial (PARADIGM-HF). Eur J Heart Fail 2013;15:1062–73.
[10] McMurray JJ, Packer M, Desai AS, Gong J, Lefkowitz MP, Rizkala AR, et al. Angiotensin-neprilysin inhibition versus enalapril in heart failure. N Engl J Med 2014;371:993–1004.
[11] Yancy CW, Jessup M, Bozkurt B, Butler J, Casey Jr DE, Colvin MM, et al. 2016 ACC/AHA/HFSA focused update on new pharmacological therapy for heart failure: an update of the 2013 ACCF/AHA Guideline for the Management of Heart Failure: a report of the American College of Cardiology/American Heart Association Task Force on Clinical Practice Guidelines and the Heart Failure Society of America. J Am Coll Cardiol 2016;68:1476–88.
[12] Velazquez EJ, Morrow DA, DeVore AD, Duffy CI, Ambrosy AP, McCague K, et al. Angiotensin-neprilysin inhibition in acute decompensated heart failure. N Engl J Med 2019;380:539–48.
[13] Ciechanover A. Intracellular protein degradation from a vague idea through the lysosome and the ubiquitin-proteasome system and on to human diseases and drug targeting: Nobel Lecture, December 8, 2004. Ann N Y Acad Sci 2007;1116:1–28.
[14] Schlossarek S, Carrier L. The ubiquitin-proteasome system in cardiomyopathies. Curr Opin Cardiol 2011;26:190–5.
[15] Mizushima N, Levine B, Cuervo AM, Klionsky DJ. Autophagy fights disease through cellular self-digestion. Nature 2008;451:1069–75.
[16] Mearini G, Schlossarek S, Willis MS, Carrier L. The ubiquitin-proteasome system in cardiac dysfunction. Biochim Biophys Acta 2008;1782:749–63.
[17] Zheng Q, Wang X. Autophagy and the ubiquitin-proteasome system in cardiac dysfunction. Panminerva Med 2010;52:9–25.
[18] Day SM. The ubiquitin proteasome system in human cardiomyopathies and heart failure. Am J Physiol Heart Circ Physiol 2013;304:H1283–93.
[19] Zech ATL, Singh SR, Schlossarek S, Carrier L. Autophagy in cardiomyopathies. Biochim Biophys Acta, Mol Cell Res 2020;1867:118432.
[20] Maejima Y. The critical roles of protein quality control systems in the pathogenesis of heart failure. J Cardiol 2020;75:219–27.
[21] Weekes J, Morrison K, Mullen A, Wait R, Barton P, Dunn MJ. Hyperubiquitination of proteins in dilated cardiomyopathy. Proteomics 2003;3:208–16.
[22] Birks EJ, Latif N, Enesa K, Folkvang T, Luong le A, Sarathchandra P, et al. Elevated p53 expression is associated with dysregulation of the ubiquitin-proteasome system in dilated cardiomyopathy. Cardiovasc Res 2008;79:472–80.
[23] Predmore JM, Wang P, Davis F, Bartolone S, Westfall MV, Dyke DB, et al. Ubiquitin proteasome dysfunction in human hypertrophic and dilated cardiomyopathies. Circulation 2010;121:997–1004.
[24] Depre C, Wang Q, Yan L, Hedhli N, Peter P, Chen L, et al. Activation of the cardiac proteasome during pressure overload promotes ventricular hypertrophy. Circulation 2006;114:1821–8.
[25] Tsukamoto O, Minamino T, Okada K, Shintani Y, Takashima S, Kato H, et al. Depression of proteasome activities during the progression of cardiac dysfunction in pressure-overloaded heart of mice. Biochem Biophys Res Commun 2006;340:1125–33.
[26] Schlossarek S, Englmann DR, Sultan KR, Sauer M, Eschenhagen T, Carrier L. Defective proteolytic systems in Mybpc3-targeted mice with cardiac hypertrophy. Basic Res Cardiol 2012;107:1–13.
[27] Thottakara T, Friedrich FW, Reischmann S, Braumann S, Schlossarek S, Kramer E, et al. The E3 ubiquitin ligase Asb2beta is downregulated in a mouse model of hypertrophic cardiomyopathy and targets desmin for proteasomal degradation. J Mol Cell Cardiol 2015;87:214–24.
[28] Zhu H, Tannous P, Johnstone JL, Kong Y, Shelton JM, Richardson JA, et al. Cardiac autophagy is a maladaptive response to hemodynamic stress. J Clin Invest 2007;117:1782–93.
[29] De Meyer GR, De Keulenaer GW, Martinet W. Role of autophagy in heart failure associated with aging. Heart Fail Rev 2010;15:423–30.
[30] Xiao R, Teng M, Zhang Q, Shi XH, Huang YS. Myocardial autophagy after severe burn in rats. PLoS One 2012;7:e39488.
[31] Mosqueira D, Mannhardt I, Bhagwan JR, Lis-Slimak K, Katili P, Scott E, et al. CRISPR/Cas9 editing in human pluripotent stem cell-cardiomyocytes highlights arrhythmias, hypocontractility, and energy depletion as potential therapeutic targets for hypertrophic cardiomyopathy. Eur Heart J 2018;39:3879–92.
[32] Feyen DAM, McKeithan WL, Bruyneel AAN, Spiering S, Hormann L, Ulmer B, et al. Metabolic maturation media improve physiological function of human iPSC-derived cardiomyocytes. Cell Rep 2020;32:107925.
[33] Schlossarek S, Singh SR, Geertz B, Schulz H, Reischmann S, Hubner N, et al. Proteasome inhibition slightly improves cardiac function in mice with hypertrophic cardiomyopathy. Front Physiol 2014;5:484.
[34] Hughes CS, Moggridge S, Muller T, Sorensen PH, Morin GB, Krijgsveld J. Single-pot, solid-phase-enhanced sample preparation for proteomics experiments. Nat Protoc 2019;14:68–85.
[35] Pankiv S, Clausen TH, Lamark T, Brech A, Bruun JA, Outzen H, et al. p62/SQSTM1 binds directly to Atg8/LC3 to facilitate degradation of ubiquitinated protein aggregates by autophagy. J Biol Chem 2007;282:24131–45.
[36] Nakamura S, Yoshimori T. New insights into autophagosome-lysosome fusion. J Cell Sci 2017;130:1209–16.
[37] Johansson M, Ulfenborg B, Andersson CX, Heydarkhan-Hagvall S, Jeppsson A, Sartipy P, et al. Cardiac hypertrophy in a dish: a human stem cell based model. Biology open 2020:9.
[38] Kobalava Z, Kotovskaya Y, Averkov O, Pavlikova E, Moiseev V, Albrecht D, et al. Pharmacodynamic and pharmacokinetic profiles of sacubitril/valsartan (LCZ696) in patients with heart failure and reduced ejection fraction. Cardiovasc Ther 2016;34:191–8.
[39] Eiringhaus J, Wunsche CM, Tirilomis P, Herting J, Bork N, Nikolaev VO, et al. Sacubitrilat reduces pro-arrhythmogenic sarcoplasmic reticulum Ca(2+)leak in human ventricular cardiomyocytes of patients with end-stage heart failure. ESC heart failure 2020;7:2992–3002.

[40] Burke RM, Lighthouse JK, Mickelsen DM, Small EM. Sacubitril/valsartan decreases cardiac fibrosis in left ventricle pressure overload by restoring PKG signaling in cardiac fibroblasts. Circ Heart Fail 2019;12:e005565.
[41] Suematsu Y, Miura S, Goto M, Matsuo Y, Arimura T, Kuwano T, et al. LCZ696, an angiotensin receptor-neprilysin inhibitor, improves cardiac function with the attenuation of fibrosis in heart failure with reduced ejection fraction in streptozotocin-induced diabetic mice. Eur J Heart Fail 2016;18:386–93.
[42] Maloyan A, Sayegh J, Osinska H, Chua BH, Robbins J. Manipulation of death pathways in desmin-related cardiomyopathy. Circ Res 2010;106:1524–32.
[43] Pattison JS, Osinska H, Robbins J. Atg7 induces basal autophagy and rescues autophagic deficiency in CryABR120G cardiomyocytes. Circ Res 2011;109:151–60.
[44] Bhuiyan MS, Pattison JS, Osinska H, James J, Gulick J, McLendon PM, et al. Enhanced autophagy ameliorates cardiac proteinopathy. J Clin Invest 2013;123:5284–97.
[45] Choi JC, Muchir A, Wu W, Iwata S, Homma S, Morrow JP, et al. Temsirolimus activates autophagy and ameliorates cardiomyopathy caused by lamin A/C gene mutation. Sci Transl Med 2012;4:144ra02.
[46] Ramos FJ, Chen SC, Garelick MG, Dai DF, Liao CY, Schreiber KH, et al. Rapamycin reverses elevated mTORC1 signaling in lamin A/C-deficient mice, rescues cardiac and skeletal muscle function, and extends survival. Sci Transl Med 2012;4:144ra03.
[47] Singh SR, Zech ATL, Geertz B, Reischmann-Dusener S, Osinska H, Prondzynski M, et al. Activation of autophagy ameliorates cardiomyopathy in Mybpc3-targeted knockin mice. circulation. Heart failure 2017:10.
[48] Rothermel BA, Hill JA. Autophagy in load-induced heart disease. Circ Res 2008;103:1363–9.
[49] Shirakabe A, Zhai PY, Ikeda Y, Saito T, Maejima Y, Hsu CP, et al. Drp1-dependent mitochondrial autophagy plays a protective role against pressure overload-induced mitochondrial dysfunction and heart failure. Circulation 2016;133:1249–63.
[50] Evans S, Ma X, Wang X, Chen Y, Zhao C, Weinheimer CJ, et al. Targeting the autophagy-lysosome pathway in a pathophysiologically relevant murine model of reversible heart failure. JACC Basic to translational science 2022;7:1214–28.
[51] Khamis T, Alsemeh AE, Abdullah DM. Sacubitril/valsartan (LCZ696) ameliorates hyperthyroid-induced cardiac hypertrophy in male rats through modulation of miR-377, let-7 b, autophagy, and fibrotic signaling pathways. Sci Rep 2022;12:14654.
[52] Hedhli N, Lizano P, Hong C, Fritzky LF, Dhar SK, Liu H, et al. Proteasome inhibition decreases cardiac remodeling after initiation of pressure overload. Am J Physiol Heart Circ Physiol 2008;295:H1385–93.
[53] Oeing CU, Mishra S, Dunkerly-Eyring BL, Ranek MJ. Targeting protein kinase G to treat cardiac proteotoxicity. Front Physiol 2020:11.
[54] Ranek MJ, Terpstra EJM, Li J, Kass DA, Wang XJ. Protein kinase G positively regulates proteasome-mediated degradation of misfolded proteins. Circulation 2013;128:365–76.
[55] VerPlank JJS, Tyrkalska SD, Fleming A, Rubinsztein DC, Goldberg AL. cGMP via PKG activates 26S proteasomes and enhances degradation of proteins, including ones that cause neurodegenerative diseases. Proc Natl Acad Sci U S A 2020;117:14220–30.
[56] Zhang HM, Pan B, Wu PL, Parajuli N, Rekhter MD, Goldberg AL, et al. PDE1 inhibition facilitates proteasomal degradation of misfolded proteins and protects against cardiac proteinopathy. Sci Adv 2019:5.
[57] Tam K, Richards DA, Aronovitz MJ, Martin GL, Pande S, Jaffe IZ, et al. Sacubitril/valsartan improves left ventricular function in chronic pressure overload independent of intact cyclic guanosine monophosphate-dependent protein kinase I alpha signaling. J Card Fail 2020;26:769–75.
[58] D'Elia E, Iacovoni A, Vaduganathan M, Lorini FL, Perlini S, Senni M. Neprilysin inhibition in heart failure: mechanisms and substrates beyond modulating natriuretic peptides. Eur J Heart Fail 2017;19:710–7.
[59] Gros C, Souque A, Schwartz JC, Duchier J, Cournot A, Baumer P, et al. Protection of atrial natriuretic factor against degradation: diuretic and natriuretic responses after in vivo inhibition of enkephalinase (EC 3.4.24.11) by acetorphan. Proc Natl Acad Sci U S A 1989;86:7580–4.
[60] Northridge DB, Jardine AG, Alabaster CT, Barclay PL, Connell JM, Dargie HJ, et al. Effects of UK 69 578: a novel atriopeptidase inhibitor. Lancet 1989;2:591–3.
[61] Bevan EG, Connell JM, Doyle J, Carmichael HA, Davies DL, Lorimer AR, et al. Candoxatril, a neutral endopeptidase inhibitor: efficacy and tolerability in essential hypertension. J Hypertens 1992;10:607–13.
[62] Stangl K, Stangl V. The ubiquitin-proteasome pathway and endothelial (dys) function. Cardiovasc Res 2010;85:281–90.
[63] Li XL, Zhu Q, Wang QC, Zhang QG, Zheng YR, Wang LH, et al. Protection of sacubitril/valsartan against pathological cardiac remodeling by inhibiting the NLRP3 inflammasome after relief of pressure overload in mice. Cardiovasc Drug Ther 2020;34:629–40.
[64] Perez-Riverol Y, Bai J, Bandla C, Garcia-Seisdedos D, Hewapathirana S, Kamatchinathan S, et al. The PRIDE database resources in 2022: a hub for mass spectrometry-based proteomics evidences. Nucleic Acids Res 2022;50. D543-D52.